Design of high-resolution variable size spatial filter for Gemini Planet Imager using flexure elements

Vlad Reshetov, Joeleff Fitzsimmons, Herzberg Institute of Astrophysics
National Research Council Canada
5071 West Saanich Rd, Victoria BC.

ABSTRACT

This paper presents a design of a variable size spatial filter used in the wavefront sensor subsystem of the Gemini Planet Imager instrument. It describes an adjustable mechanism consisting of two slides forming a square aperture which can be varied in size between 1.8 and 6.7 mm. These slides are located on athermalized flexure mounts that move opposite to one another driven by a single precision linear actuator. The device retains long term dimensional stability, resolution, and repeatability on a micron level for all gravity vector orientations and for temperatures between -5°C and + 25°C.

Keywords: spatial filter, athermalization, double parallelogram flexure.

1. INTRODUCTION

The Gemini Planet Imager (GPI) instrument is currently under construction and will be deployed in 2010 on the Gemini South telescope. With contrast levels on the order of 10^{-7} to 10^{-8} this instrument will allow for the direct observation of self-luminous extrasolar planets at near infrared wavelengths [1].

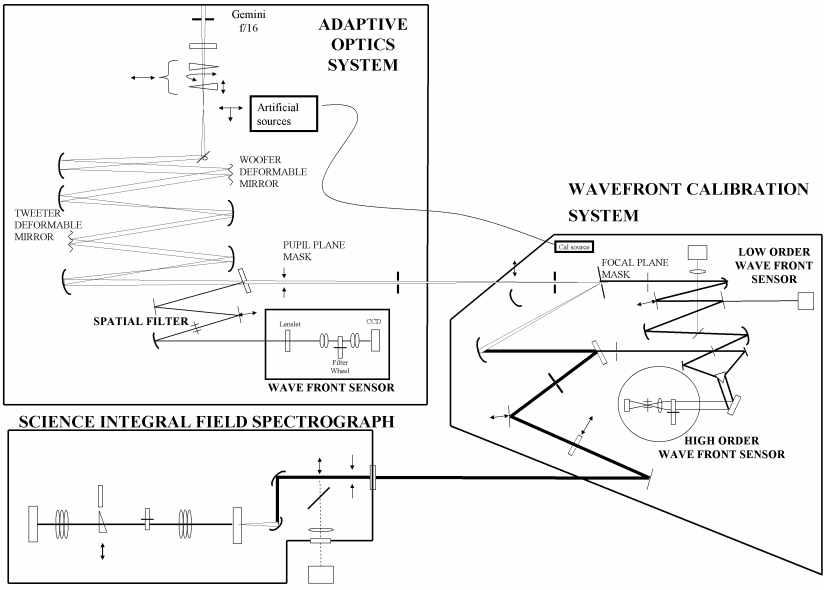

Fig. 1. GPI functional layout [4].

The functional layout of the instrument is presented on Fig. 1. The GPI consists of four subsystems: the Adaptive Optic System (fast wavefront sensor and wavefront control); coronagraph (focal plane mask and pupil apodization – on the diagram shared between the adaptive optic system and the wavefront calibration system); integral field spectrograph (science instrument); and the wavefront calibration system [2].

The adaptive optics module is based on the Shack–Hartmann method. The wavefront sensor camera assembly includes the lenslet array, the reimaging doublets, the filter changer and the CCD. It operates over a bandpass of 700–900 nm. Wavefront distortions, as measured by the lenslet array, are fed back into the low frequency deformable mirror (woofer) and the high spatial frequency deformable mirror (tweeter) for compensation. The spatial filter is located in the input focal plane of the wavefront sensor. The function of the spatial filter is to attenuate aliasing errors. Aliasing errors are caused by the wavefront sensor interpreting high spatial frequency wavefront distortions as low frequency ones, and compensating for them. The spatial filter serves as a low-pass filter, by reducing the power of high spatial frequency signals. Further details on the theory behind the introduction of the spatial filter into the wavefront sensor beam path can be found in [3].

2. MECHANICAL SPECIFICATIONS AND CONSTRAINTS

The mechanical function of the wavefront sensor spatial filter is to vary the size of a square aperture allowing more or less of the image plane to pass through to the wavefront sensor camera.

Geometry specifications:

- The square aperture must be variable in size to accommodate different observing conditions.
- The side dimension of the square aperture will vary for normal observing requirements as follows:
    - Minimum width = 0.7 arcsec or 1.75 mm (for 700 nm wavefront sensor band);
    - Maximum width = 2.0 arcsec or 5.00 mm (for 900 nm wavefront sensor band);
- The total side dimension range will be 1.75 mm to 6.72 mm. The maximum opening of 6.72 mm is derived from the wavefront sensor system having a scale of 2.4 mm/arcsec (f/64 beam) combined with the ‘wide-open’ configuration of 2.8 arcsec.

Resolution and repeatability requirements (within -5 to 25°C temperature range):

- The square aperture must be adjustable to increments of 47μm. Positioning within 10% of these increments, or 4.7μm, leads to the following resolution and repeatability requirements:
- Size resolution of ±4μm (goal: ±2μm)
- Size repeatability of ±16μm (goal: ±8μm)
- Size stability for 15 degrees telescope motion or 1 hour of elapsed time ±10μm (goal: ±5μm)
- Over the entire range of motion, the square aperture shall not rotate more than 10 mrad or decenter more than 19μm.

- Adjacent sides of the square pin-hole must remain within 5 mrad perpendicular to one another.
- The gap between adjacent sides of the square aperture should not exceed 0.3 mm

The time required for the full-range adjustment of the square pin-hole had to be less than 5 seconds with the goal of 2 seconds. Because the controller for other actuators was already selected in the instrument, the actuator needed to be DC motor based. The linear optical encoders, common on many commercially available linear stages, can not be used in this instrument. There is a danger that light sources on such encoders will create stray light right in the 700 – 900 nm band we are trying to measure. Given the sensitivity of the measurement, stray light suppression techniques were deemed to introduce additional risk and complexity.

3. SELECTION OF THE DESIGN CONCEPT

Given that no kind of feedback can be derived from the instrument on the position and the size of the spatial filter aperture, the most critical requirements are size repeatability (±16μm with the goal of ±8μm) and decentering (< 19μm). The importance of the size repeatability requirement can be illustrated as follows. The optical bench of the instrument, the brackets and the mounts for other optical elements are all made from the same material, aluminum, to match thermal expansion. The most straightforward way of implementing the spatial filter would be to use two opposing off-the-shelf commercially available linear stages. However, for a typical aluminum stage with a steel lead screw, the difference in the thermal expansion on a 30 mm length of lead screw over the temperature range of 30°, will already be equal to 10 μm. If we add the typical ±3 μm (repeatability without a linear encoder) per each of the two stages, and if we add another ± 3 μm of initial alignment error, we get ± 14 μm of total repeatability as compared to ±16 μm specified as maximum. This is with offsetting the zero point of room temperature alignment by half of our expected thermal expansion, and not counting the thermal expansion of the material of aperture leafs. The leafs, if made from aluminum, will contract by 3.9 μm over the operating temperature range. It is quite clear that an athermalization of the actuation mechanism will be necessary. This can be accomplished by an active temperature compensation (temperature table) or passively, by utilizing athermalized mounts. Use of the active compensation, such as temperature tables, to compensate for thermal drift should to be avoided (and kept as an option of last resort) as it increases the complexity and reduces the overall reliability of the system. Therefore the athermalized design would be the preferred way to deal with the temperature variations.

Conceptually the spatial filter mechanism should consist from three functional parts: two linear guides carrying aperture leafs, an actuator (or actuators), and an interface between the linear guides and an actuator. This interface should include a reversing lever to drive both linear guides in the opposing directions simultaneously. Flexure-based translational guides were chosen for a number of reasons: they are easy to athermalize, there is no sliding friction which can result in stick-slip conditions, they are easy to fit into the spatial envelope allowed for this subassembly and, finally, there is no wear. Similar translational guide design was used by R. V. Jones in optical slit mechanism [5].

The most logical choice for the reversing lever pivot would have been to employ a flexure pivot. It has the same advantages as a flexure-based linear guide, but rather a large rotation (12°) of the reversing lever makes the use of flexure pivots less attractive. Relatively low stiffness of the flexure pivots combined with substantial parasitic center shift causes parasitic translation of the aperture to be uncomfortably close to the decentering limit of 19 μm. Therefore a ball bearing pivot was selected.

4. DETAILED DESCRIPTION OF THE DESIGN

4.1 Principle of operation

The wavefront sensor spatial filter consists of a square aperture that is adjustable between the maximum and the minimum size while remaining centered on the optical path. As illustrated in Fig. 2, the adjustable mechanism consists of two opposing leafs mounted on the leaf carriers, and driven by a single precision linear actuator. Leaf carriers and the actuator are mounted onto an L-shaped top bracket.

The reversing lever is located under the leaf carrier blocks, and is mounted to the same L-shaped top bracket. It is connected to the leaf carriers via flat flexible links.

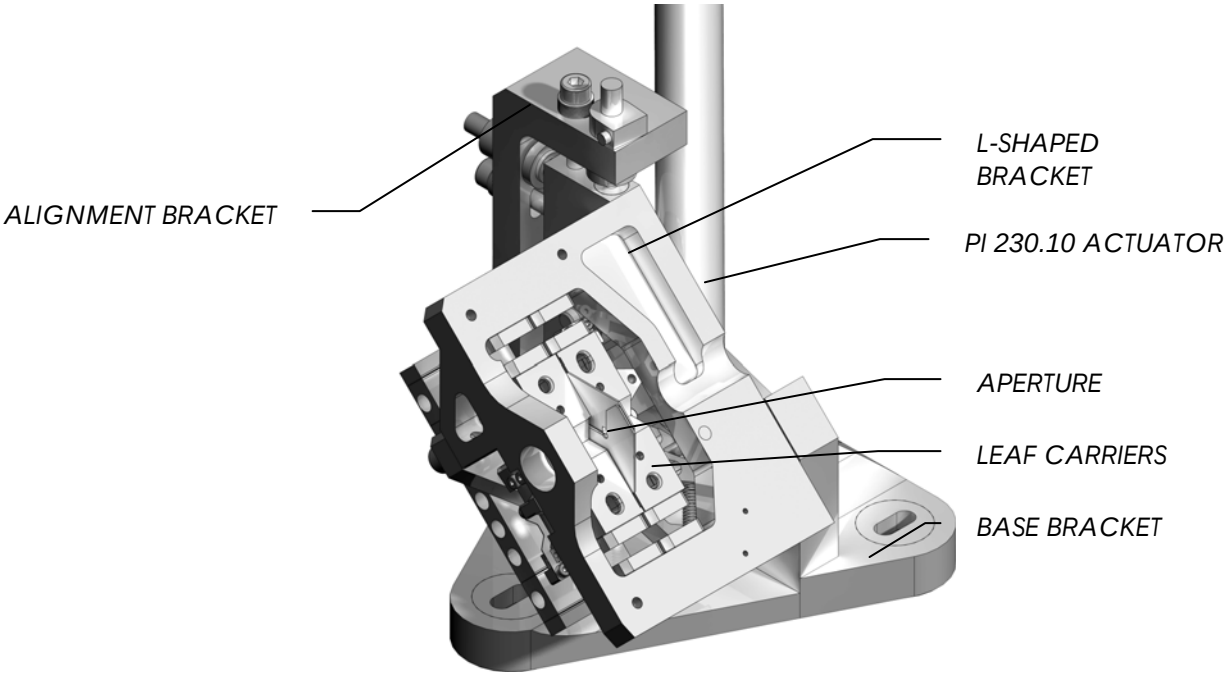

Fig. 2. Overall view of the assembly.

4.2 Translational guides

Translational guides are shown in Fig. 3. This configuration has been described in various sources [5] and is known as double parallelogram flexure [6]. An actuation force is applied at the leaf carrier platform (shown on top). It moves it in a straight line along the X axis. The block shown on the bottom – the auxiliary block – translates half of distance traveled by the leaf carrier block. This

configuration offers several important advantages over the more simple arrangement known as the parallelogram flexure.

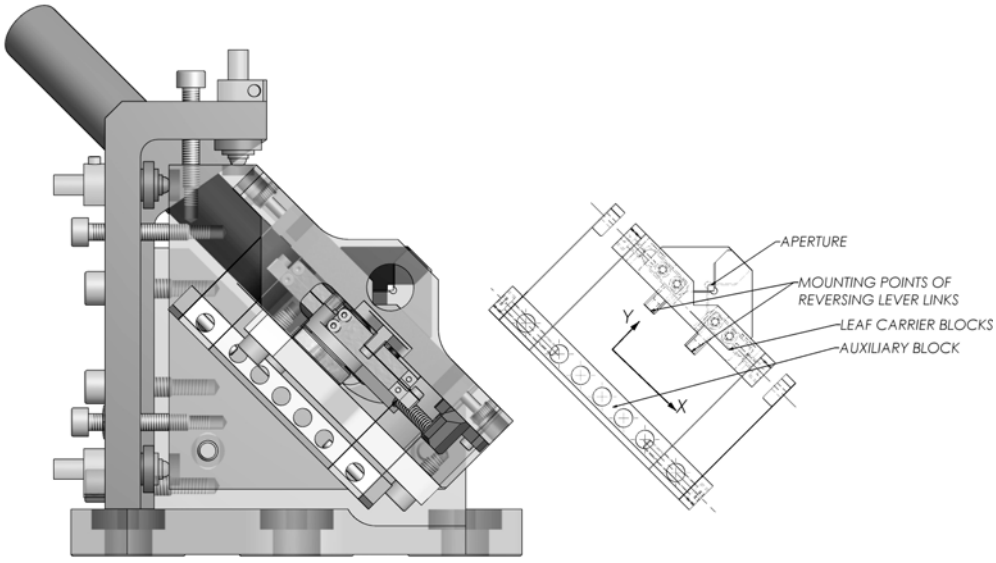

Fig. 3. Translational guides.

First of all, it does not suffer from parasitic motion along the Y axis. Such motion follows a path with a radius roughly equal to the length of flexures. In the double parallelogram arrangement shown on Fig. 3, the distance between the leaf carrier and the auxiliary blocks changes as the leaf carrier block moves, but the leaf carrier itself - in an ideal case - moves in a straight line.

The second advantage is athermalization in the Y direction. The position of the guide block does not change with temperature relative to the support bracket. Expansion or contraction of the flexures result only in the movement of the auxiliary block relative to the leaf carrier block.

The third advantage of the double parallelogram arrangement is that it allows for a more compact design: each flexure deflects only half of the total range of motion; therefore they can be made shorter. The length of the flexures is determined from the condition that maximum stress should not exceed fatigue limit. Therefore for a given travel and flexure thickness there is a minimum flexure length, and it can be calculated as follows:

From [7] for each individual flexure the deflection will be equal to

$$\delta = \frac{W \cdot L^3}{12 \cdot E \cdot I} \tag{1}$$

Where: W – actuation force, L – length of the flexure, E –Young's modulus, I – flexure section moment of inertia. Moment of inertia is equal to

$$I = \frac{b \cdot h^3}{12} \tag{2}$$

Substituting (2) into (1) and solving for actuation force, W gives us

$$W = \frac{\delta}{L^3} \cdot E \cdot b \cdot h^3 \tag{3}$$

Maximum bending moment in the flexure [7]:

$$M_{max} = \frac{W \cdot L}{2} \tag{4}$$

Maximum stress in the flexure:

$$\sigma_{max} = \frac{M_{max}}{\left(\frac{b \cdot h^2}{6} \right)} \tag{5}$$

After substituting expressions for maximum bending moment (4), and actuation force (3) into (5) we will get:

$$\sigma_{max} = 3 \cdot \frac{\delta}{L^2} \cdot E \cdot h \tag{6}$$

If we limit maximum stress of the flexures to be below the fatigue limit (σ_f), we can find the minimum length of the flexures from the expression (6). The formula for the minimum length of the flexures at which maximum stress will not exceed the fatigue limit for a given travel:

$$L_{min} = \frac{1}{\sigma_f} \cdot \sqrt{3 \cdot \left(\sigma_f \cdot \delta E \cdot h \right)} \tag{7}$$

Knowing that the fatigue strength of half-hard 304 stainless steel will be 0.35 (asymmetrical loading cycle [8]) of the tensile strength of 1035 MPa, and thus be equal to 362 MPa, and the range of motion of an individual flexure will be half of the range of the motion of the leaf carrier block or 1.8 mm, we can find the minimum length of 0.2 mm thick flexures from formula (7) to be equal to 24.1 mm. In the actual design, the length of the flexures was chosen to be 29 mm, this implies a safety factor of 1.45 in terms of fatigue strength.

To reduce parasitic motions the construction of the translation mechanism must meet several important conditions: all blocks should have the same length, and preferably machined together. Length of the flexures should be as equal as possible, therefore during assembly leaf carrier blocks and auxiliary blocks will be spaced from each other with gage blocks. Fillets on the clamps and on the blocks (at the corners where flexures are clamped to blocks) help to decrease stress concentration and to alleviate the uncertainty associated with the exact line of contact between clamps or blocks and the flexures.

4.3 Actuation mechanism

Assembly is actuated by a single off-the-shelf commercial actuator: Physik Instrumente M230.10 DC high-resolution closed-loop DC-mike type. It consists of a micrometer with a non-rotating tip driven by a closed-loop DC motor with 42.92:1 gearhead, and with a motor-shaft-mounted, high-resolution encoder (2048 counts/rev.).

As shown in Fig. 4, the reversing lever is preloaded against the actuator with a compression spring. The contact pair between the actuator and the lever is a tungsten carbide ball on a tungsten carbide insert (4 mm diameter tungsten carbide ball and RNM22S0820 KB9640, Kendex negative solid PCBN insert). The reversing lever is suspended on two ABEC 9 bearings from Barden Inc. They are preloaded on the shaft using belleville washers. The material of the actuation lever and of the actuation shaft is stainless steel 420. It was chosen to match the thermal expansion coefficient of ball bearings (10 ppm per °C). Transfer of the actuation force from the lever to the slides is accomplished via double flat flexure links (Fig. 5). The intent here is to constrain only one degree of freedom and effectively decouple linear slides from parasitic motions of the reversing lever. An advantage of such configuration is that it is mostly athermalized because it forms a loop. The thinner, more compliant flexure will be wrapping around the reversing lever on 40 mm diameter, 12° of rotation as the aperture opens. With the bend radius being relatively small, having the flexure thin allows us to keep mechanical stress below the fatigue limit.

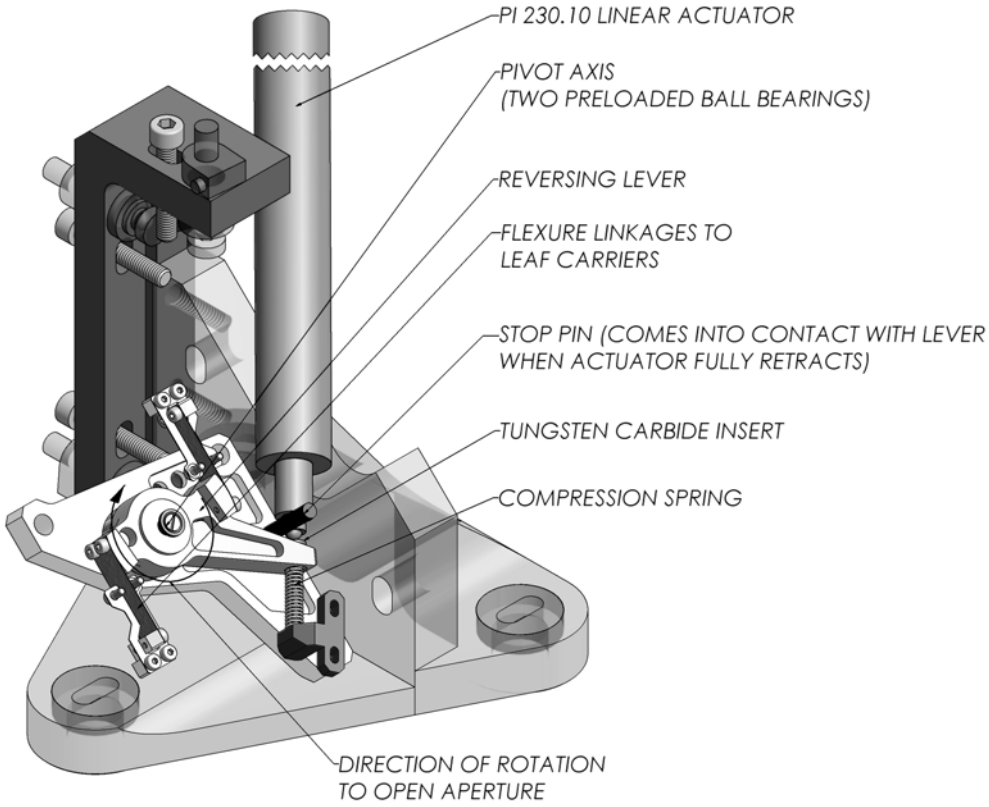

Fig. 4. Reversing lever system (L-shaped bracket and leaf carriers are not shown).

Throughout the operating range, forces acting through the flexure links are always applied in only one direction. The zero strain point of the double parallelogram flexures corresponds to an aperture slightly smaller than the minimum aperture. Therefore the thin flexures experience only tensile stress and are not subject to buckling. The critical load of the flexure working in compression is calculated to be 40 N, or four times the maximum expected load. It is parallel to the plane of rotation of the reversing lever. It is expected that the reversing lever will rotate parallel (within machining tolerances) to the plane of translation of the leaf carrier blocks, and will have minimal parasitic displacements.

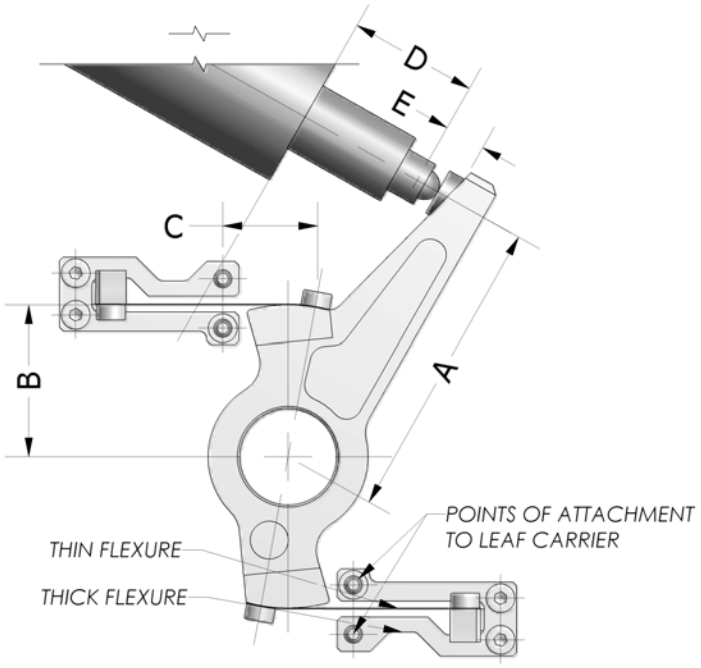

Fig. 5. Athermalized linkages between reversed lever system and translational guides.

4.4 Assembly and alignment on the instrument

The assembly will be aligned to mechanical references on the instrument using an NC measuring machine. Sides of the aperture are to be used as datums. Adjustment will be achieved by translating the mounting surfaces (flat on flat) in relation to each other. For instance, the L-shaped bracket will allow alignment in three degrees of freedom: translations along X and Y and rotation around Z (Fig. 6). The base bracket will allow translations and rotation in XZ plane.

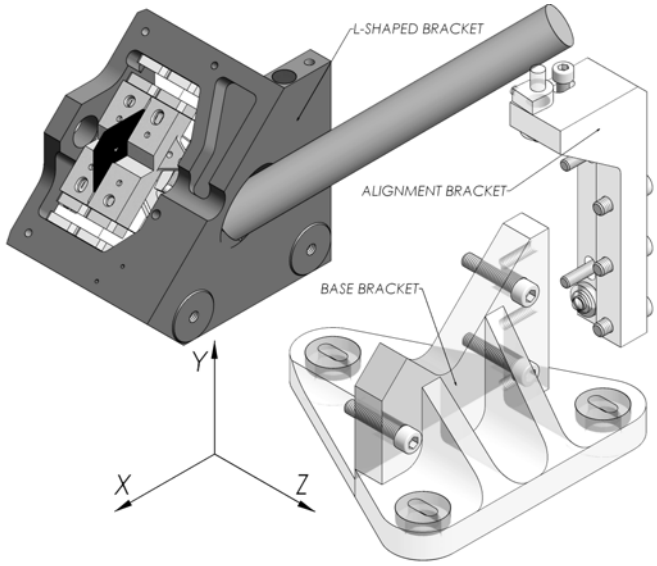

Fig. 6. Alignment of the spatial filter on the instrument.

5. EXPECTED PERFORMANCE

5.1 Balance of thermal expansions/contractions in the actuation loop

With an operating temperature range of the instrument of 30 degrees, from -5°C to +25°C, balance of thermal expansions/contractions is critical to the performance. This balance can be estimated with the help of Fig. 5.

With a drop in temperature the reversing lever (distance B), and distance from the pivot point to the actuator (distance A), will contract at different rates. On balance this will increase the transfer ratio between the actuator and the aperture size (the actuator moves with the aluminum of L-shaped bracket, but the steel of the reversing lever contracts less). This will result in the aperture opening by an extra 2.6 μm:

$$6.72 \cdot mm \cdot \frac{2 \cdot \left(20 \cdot mm - 20 \cdot mm \cdot 10.3 \cdot 10^{-6} \cdot K^{-1} \cdot 30 \cdot K\right)}{40 \cdot mm - 40 \cdot mm \cdot 23 \cdot 10^{-6} \cdot K^{-1} \cdot 30 \cdot K} - 6.72 \cdot mm = 2.562 \ \mu m$$

Contraction of the aperture due to differential thermal expansion of the links (distance C):

$$-2 \cdot 12.5 \cdot mm \cdot (23 - 17.3) \cdot 10^{-6} \cdot K^{-1} \cdot 30 \cdot K = -4.275 \ \mu m$$

Expansion of the aperture due to differential thermal expansion of the actuator (steel actuator tip vs. aluminum mounting bracket, distance D):

$$17 \cdot mm \cdot \left[(23 - 12) \cdot 10^{-6} \cdot K^{-1} \cdot 30 \cdot K\right] = 5.61 \ \mu m$$

Expansion of the aperture due to differential thermal expansion between the aluminum and the contact couple of tungsten carbide actuator tip and hard insert (distance E):

$$6.1 \cdot mm \cdot \left[(23 - 5.1) \cdot 10^{-6} \cdot K^{-1} \cdot 30 \cdot K\right] = 3.276 \ \mu m$$

Contraction of the aperture due to the contraction of the leafs (not shown on the picture):

$$-6.72 \cdot mm \cdot \left[23 \cdot 10^{-6} \cdot \left(K^{-1} \cdot 30 \cdot K\right)\right] = -4.637 \ \mu m$$

With 30° temperature drop the aperture will expand by:

$$(2.562 - 4.275 + 5.61 + 3.276 - 4.637) \cdot \mu m = 2.536 \ \mu m$$

5.2 Overall error budget

The variation in the aperture size will be mostly caused by three factors: actuator repeatability (±3 μm), thermal expansion of the actuation loop (+2.5 μm, as calculated in the previous paragraph), and the initial alignment and calibration (± 3 μm). The total expected error on the size of the aperture will be within ±7.25 μm with a specified repeatability goal being ± 8 μm. Errors from changes in gravity orientation are expected to be comparatively small.

Decentering error will mostly result from an inexact placement of the reversing lever in relation to its center of rotation. Position of the center of rotation will depend on manufacturing tolerances and on the bearing runout. The bearing runout contributes to the translation of the aperture directly and is assumed to be ±3 μm. Manufacturing tolerances on the reversing lever assembly (unequal leverage)

are contributing ± 2 μm over 7 mm of overall travel. So, total decentering is expected to be less then ± 5 μm. This is well within the 19 μm of maximum decentering specified.

REFERENCES

[1] Macintosh, B., et al., "The Gemini Planet Imager," Proc. SPIE 6272, 18, (2006).

[2] Graham, J. R., Macintosh, B., "Operational Concept Definition Document," GPI internal document, 52, (2006).

[3] Poyneer, L. A. and Macintosh B., "Spatially filtered wave-front sensor for high-order adaptive optics," J. Opt. Soc. Am. A, Vol. 21, No. 5, 810-819 (2004)

[4] Saddlemyer L., "GPI System sketch," GPI internal document, 1, (2008).

[5] Jones R. V., "Instruments and Experiences: Papers on Measurement and Instrument Design," John Wiley & Sons, 105-116, (1988).

[6] Awtar S., "Synthesis and Analysis of Parallel Kinematic XY Flexure Mechanisms," Sc.D. Thesis, Mass. Inst. Tech., 42, (2003).

[7] Young W. C., "Roark's Formulas for Stress and Strain," Mcgraw-Hill, (1989).

[8] Johansson R., Nordberg H., "Fatigue Properties of Stainless Steel Strip," http://www.outokumpu.com, (2002).